Chapter 5

Galactic Cosmic Ray Energy Losses and Propagation Times

5.1 Introduction

The ability of SDE based numerical modulation models in calculating CR intensities was shown in the previous chapter. SDE type models also allow for the calculation of CR propagation times (some authors refer to this as the residence or transit time; i.e. the time a CR takes to propagate from its source to some observational point in the heliosphere) and energy losses, directly from the numerical scheme. The methodology of calculating these quantities using an SDE model, as well as the accuracy of the solutions, is discussed in this chapter, where after these quantities are calculated for GCR protons and electrons in successive solar cycles. Propagation times are also calculated in Chapters 6 and 7, and as such, this chapter serves as an introduction to those chapters.

The propagation times of CRs have been a topic of study since *Parker* [1965] derived his original TPE. These analytical calculations were revisited by *O'Gallagher* [1975], who essentially found the propagation time to be energy dependent (more precisely, to be dependent on the diffusion coefficient, normally taken to be energy dependent), with longer propagation times for lower energy particles. This time-lag of CRs in responding to changing modulation conditions can explain the observed hysteresis effect in CR intensities as observed at Earth [e.g. *O'Gallagher*, 1975; *Kane*, 1981]. Recently, *Florinski and Pogorelov* [2009] demonstrated the advantage of SDE type models by calculating the propagation times of CRs in a geometrically realistic 3D heliosphere, finding long propagation times for CRs in the turbulent heliosheath region. Interpreting the longer propagation time in this region as an indication of large amounts of energy being lost (via adiabatic cooling) by CRs, is incorrect. The relation between the propagation times and energy losses is investigated further in this chapter.

Similarly, the energy losses suffered by CRs propagating through the heliosphere have been studied extensively in the past, both theoretically [e.g. *Parker*, 1965; *Parker*, 1966; *Jokipii and Parker*, 1965; *Webb and Gleeson*, 1979, 1980] and observationally [e.g. *Gleeson and Palmer*, 1971;

Urch and Gleeson, 1973], as well as through numerical modulation models [e.g. *Goldstein et al.*, 1970; *Moraal and Potgieter*, 1982; *Zhang*, 1999]. *Zhang* [1999] also illustrated the applicability of SDE type models in calculating this quantity. By examining these energy losses, insight can be gained about e.g. the effect of adiabatic cooling on the modelled and observed CR spectral shapes, as well as relating low energy CRs at Earth with their higher energy counterparts in the outer heliosphere.

The results of this chapter are summarized in *Strauss et al.* [2011b].

5.2 Calculating Cosmic Ray Propagation Times and Energy Losses

The methodology used to calculate propagation times and energy losses is illustrated in this section, by integrating a 1D spherically symmetric version of the TPE time backwards by means of SDEs in terms of radial distance r and kinetic energy E. The integration process is started at a so-called observational point (r^0, E^0), i.e. the phase space position where the CR intensity is calculated, and continued until the boundary, set at $R = 100$ AU, is encountered at the so-called exit position (r^e, E^e). The left panel of Fig. 5.1 shows a realization of a single phase space point starting at $(r^0, E^0) = (1 \text{ AU}, 0.1 \text{ GeV})$ and ending at $(r^e, E^e) \approx (100 \text{ AU}, 0.13 \text{ GeV})$. This is done for galactic electrons with a constant diffusion coefficient of $\kappa = 80$ PUs, where PUs refers to program units (1 PU $= 6 \times 10^{20}$ cm^2.s^{-1}), introduced for shorter notation. Interpreting the bottom left panel of the figure in the traditional time forwards scenario, a pseudo-particle enters the heliosphere at $t = 0$ $(s = 58)$ days at 100 AU and propagates towards the inner heliosphere, reaching 1 AU at $t = 58$ days $(s = 0)$. Furthermore, in terms of kinetic energy (the top left panel of the figure), the pseudo-particle enters the heliosphere with $E = 130$ MeV, loosing $\Delta E = 30$ MeV adiabatically during its propagation (transit through the heliosphere), and reaching 1 AU with 100 MeV. Note that the trajectory of the pseudo-particle is smooth in terms of E, while exhibiting a stochastic nature in terms of r. This is because only spatial diffusion, and not energy diffusion, is taken into account.

The SDE approach allows for the calculation of the propagation time of CRs directly from the numerical method. For the realization of a single pseudo-particle, labelled by the index i, the propagation time is simply the time it takes for the pseudo-particle to be transported, for the 1D case, from r^0 to r^e, calculated as

$$\tau_i = \left| s_i^e - s_i^0 \right| . \tag{5.1}$$

For the scenario illustrated in the left panel of Fig. 5.1, $\tau_i = 58$ days. Calculating τ for a single pseudo-particle is, however, statistically insignificant. Therefore, τ_i is calculated for a large number of these particles (usually $N > 3000$) and binned in a normalized histogram. The expectation value is calculated as the weighted average of τ_i, as

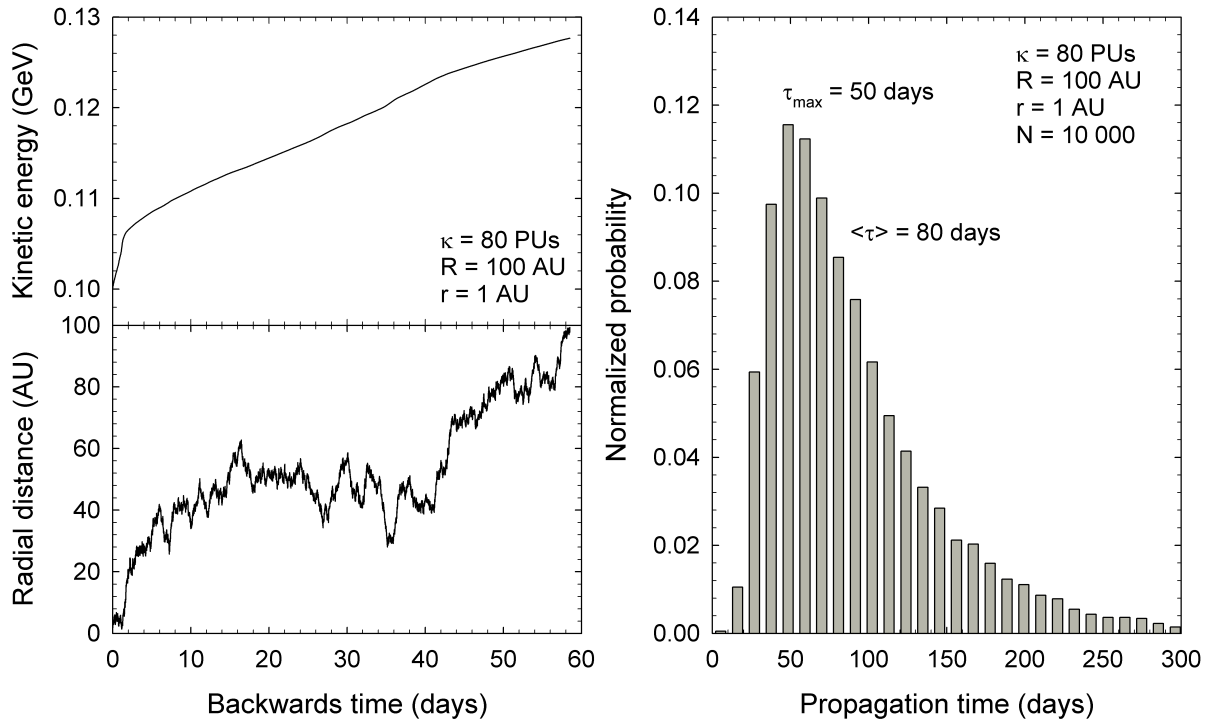

Figure 5.1: The left panel shows an example of the evolution of a phase space density element (pseudo-particle), as described by the set of SDEs (for the spatially 1D case) in terms of kinetic energy (top panel) and radial distance (bottom panel) for galactic electrons. The right panel shows the binned propagation time, constructed from $N = 10000$ pseudo-particle trajectories and by making use of Eq. 5.3.

$$\langle \tau \rangle = \sum_{l=1}^{M} \tau_l \rho_l, \tag{5.2}$$

where M refers to the number of bins in the distribution and ρ_l is the probability of finding τ_i in the time bin τ_l,

$$\rho_l = \frac{N_l}{N}, \tag{5.3}$$

with N_l the number of particles ending up in the l-th bin and the normalization condition

$$\sum_{l=1}^{M} \rho_l = 1 \tag{5.4}$$

automatically satisfied.

The right panel of Fig. 5.1 shows the normalized probability density of the propagation time, calculated for $N = 10000$ pseudo particles (in this case galactic electrons). This figure is constructed by repeating the phase-space integration illustrated in the left panel 10 000 times (each time using a different sequence of Wiener processes, i.e. each time integrating the trajectory of

a different pseudo-particle) and using Eq. 5.3 to construct the normalized probability density of the propagation time. Two timescales are indicated on the figure, namely: τ_{max} which is the most probable propagation time, and $\langle\tau\rangle$, which is the average propagation time (i.e. the expectation value thereof). Because of the long tail in the distribution of τ, one generally finds that $\langle\tau\rangle > \tau_{max}$. For the rest of this chapter only the behaviour of $\langle\tau\rangle$ is considered.

Since the time backwards approach to solve the relevant SDEs is used, the normalization to unity is characteristic of the method of solution; in the normal time forward case this corresponds to all particles entering the heliosphere, eventually reaching a point r^0 in the inner heliosphere, after some time $\tau > 0$. In later sections this normalization of the propagation time is discussed further.

Similar to $\langle\tau\rangle$, the SDE approach also allows for the direct calculation of the energy lost by a CR during its propagation through the heliosphere. Again the expectation value of the exit energy $\langle E^e\rangle$, can be calculated (in the time forward scenario, E^e would refer to the energy of a CR directly before entering the heliosphere). The average amount of energy loss during the propagation process is then

$$\langle\Delta E\rangle = \langle E^e\rangle - E^0. \tag{5.5}$$

5.3 Electrons and Protons in One Dimension

5.3.1 Case 1: A Diffusion Dominated Scenario

In his seminal paper, *Parker* [1965] introduced the probability wave approach to study the propagation times of CRs. Instead of computing the differential intensity of the CRs, this approach calculates the probability $w(r,t)$ of finding a particle at a position r at a time t. Choosing a constant (energy and spatially independent) diffusion coefficient in 1D, the processes that influence CR transport are convection and diffusion. The evolution of $w(r,t)$ thus satisfies the convection-diffusion Fokker-Planck equation

$$\frac{\partial w(r,t)}{\partial t} = \frac{1}{r^2}\frac{\partial}{\partial r}\left(r^2\kappa\frac{\partial w(r,t)}{\partial r}\right) - V_{sw}\frac{\partial w(r,t)}{\partial r}, \tag{5.6}$$

with the first term on the left hand side referring to the inward diffusion of galactic cosmic rays and the second term the outward convection by the solar wind and embedded magnetic field. As a first application of this model, the system is assumed to be diffusion dominated and convection is neglected by setting the solar wind speed to $V_{sw} = 0$. For this scenario, Eq. 5.6 can be solved analytically quite easily. As an initial condition, an empty heliosphere is assumed and the CR particles are introduced at a radial position of $r = R - h$ at $t = 0$, where R is the radius of the outer boundary (HP), and h the penetration length of a galactic CR, i.e. the distance it penetrates the heliosphere before being scattered for the first time. With these

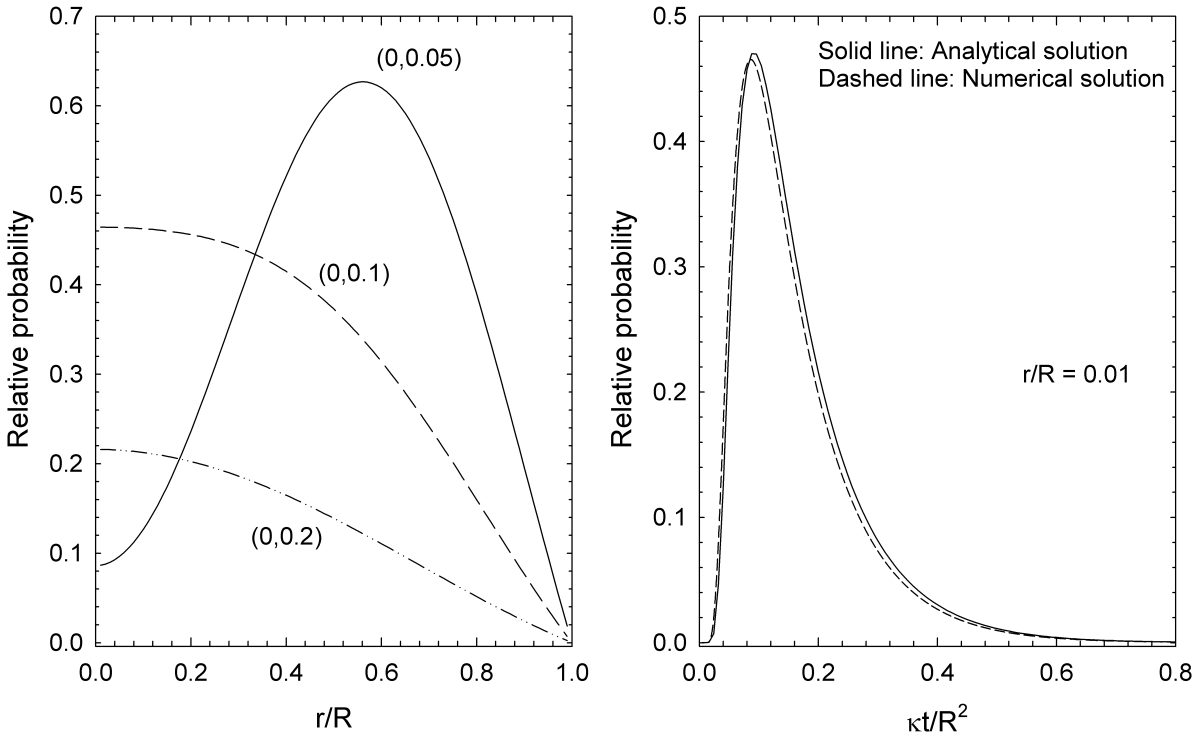

Figure 5.2: The left panel shows $w(r,t)$ as a function of radial distance. The curves are labelled by values for $(RV_{sw}/\kappa, \kappa t/R^2)$ with $V_{sw} = 0$ when convection is neglected. The right panel shows the temporal evolution of $w(r,t)$ at a fixed spatial point. The solid line is the analytical solution of Eq. 5.6, while the dashed line is a numerical solution of the same equation.

assumptions, using a free-escape outer boundary (CRs are free to leave the heliosphere) and a reflecting inner boundary at $r = 0$, *Parker* [1965] obtained

$$w(r,t) \approx \frac{h}{2R^3 r} \sum_{n=1}^{\infty} (-1)^{n-1}\, n \sin\left(\frac{n\pi r}{R}\right) \exp\left(-\frac{n^2\pi^2\kappa t}{R^2}\right), \tag{5.7}$$

valid for $h \ll R$. As $w(r,t)$ is a probability, it can be re-normalized to unity because of the linearity of Eq. 5.6. The left panel of Fig. 5.2 shows $w(r,t)$ as a function of normalized distance. The numbers in brackets label the curves according to the dimensionless parameters $(RV_{sw}/\kappa, \kappa t/R^2)$. Assuming κ and R to be constant, the curves can be interpreted as showing the temporal evolution of $w(r,t)$. Starting from an initial delta function, the probability wave diffuses spatially, getting reflected at the inner boundary, and finally being absorbed at the outer boundary. The right panel of Fig. 5.2 shows the temporal evolution of $w(r,t)$ at a constant radial position of $r/R = 0.01$ (i.e. 1 AU for this choice of R). Starting from zero at $t = 0$, the probability of finding a particle at this position increases sharply to a maximum (the most probable propagation time), whereafter it decreases again to zero, following an almost Poisson like distribution.

The expectation value $\langle\tau\rangle$, of the propagation time is calculated, for a particular spatial point

$r_a < R$, as

$$\langle \tau \rangle = \frac{\int_{t=0}^{\infty} w(r_a, t) t dt}{\int_{t=0}^{\infty} w(r_a, t) dt}. \tag{5.8}$$

Again this equation can be solved analytically to give

$$\langle \tau_d \rangle = \frac{R^2}{\pi^2 \kappa} \sum_{n=1}^{\infty} \frac{1}{n^2} \rightarrow \frac{R^2}{6\kappa}, \tag{5.9}$$

where the subscript d indicates that this is the average propagation time when only diffusion is considered. *O'Gallagher* [1975] derived the same expression for $\langle \tau_d \rangle$ and refers to this as the diffusion time scale. Note that $\langle \tau_d \rangle$ is inversely proportional to κ and that $\langle \tau_d \rangle \rightarrow \infty$ when $\kappa \rightarrow 0$, while $\langle \tau_d \rangle \rightarrow 0$ when $\kappa \rightarrow \infty$.

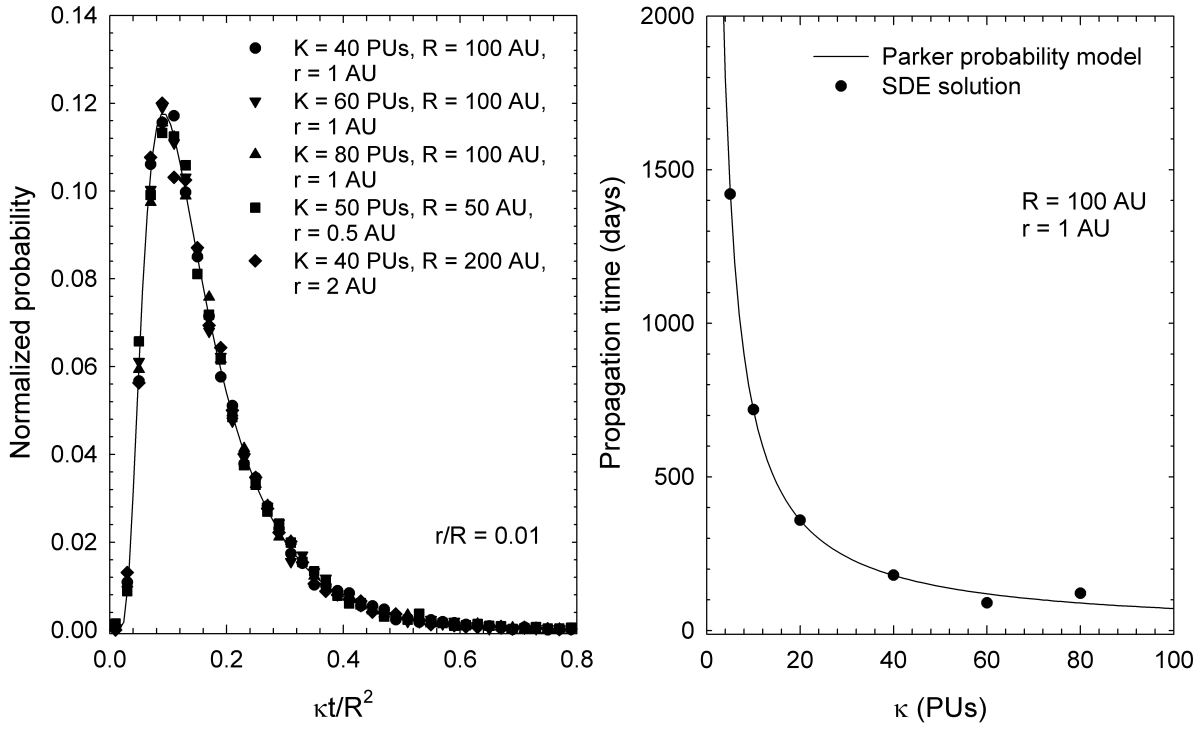

Figure 5.3: The left panel shows the binned propagation times as calculated with the SDE model for different transport parameters (scatter points) at a radial position of $r/R = 0.01$, while the solid line shows the re-normalized probability, initially shown in the right panel of Fig. 5.2. The right panel shows $\langle \tau \rangle$, as calculated with Eq. 5.9, with $R = 100$ AU, as the solid line, while the scatter points show $\langle \tau \rangle$ as a function of κ as calculated with the SDE model.

The SDE solutions shown and discussed in this paragraph neglect solar wind convection consistent with the analytical approximations discussed in the previous paragraph. The left panel of Fig. 5.3 shows the binned propagation times from the SDE model as scatter points. This is similar to the right panel of Fig. 5.1, but with the time expressed as $\kappa t/R^2$, using different

combinations of κ and R. All solutions are shown at a constant (normalized) radial position of $r_a = r/R = 0.01$. The solid line shows the analytical solution, given by Eq. 5.7, with the probability $w(r,t)$ re-normalized so that

$$\int_{t=0}^{\infty} w(r_a,t)dt = 1, \tag{5.10}$$

in line with the results from the SDE model where all CRs entering the heliosphere will penetrate up to r_a. The solutions of the SDE model compare very well with the analytical approximation, confirming the reliability of the results generated with the SDE model. In order to test the validity of Eq. 5.9, the right panel of Fig. 5.3 shows $\langle\tau\rangle$, as calculated with Eq. 5.9, as the solid line, while the scatter points show the results from the SDE model for the same scenario. Again, excellent agreement between the two methods is obtained, which can be considered as a validation of the the SDE approach in calculating $\langle\tau\rangle$.

5.3.2 Case 2: A Diffusion-Convection Scenario

The solutions of the previous paragraphs neglected the outward convection by the solar wind, which is now included. As shown by *Parker* [1965] and *O'Gallagher* [1975], analytical solutions of Eq. 5.6 are possible only for very limited cases. Therefore the probability wave equation is solved numerically, where κ is again assumed to be constant and the equation is solved by a finite-differences scheme. The right panel of Fig. 5.2 already showed the numerical solution as the dashed line, using $R = 100$ AU and $h = 15$ AU, compared to the analytical solution of *Parker* [1965] as the solid line.

In the left panel of Fig. 5.4, $w(r,t)$, as calculated numerically, is shown as a function of radial distance for varying times in days. Two solutions are shown: including convection (solid lines) and neglecting convection in the model (dashed lines). With the inclusion of outward convection, it is clear that the CRs find it more difficult to reach the inner heliosphere. The right panel of the figure shows $w(r,t)$ as a function of time at $r = 1$ AU (Earth) for the same two cases shown in the left panel. What is notable from the solutions is that τ_{max} is approximately equal for the different cases. However, the calculated distribution including convection is much wider than the case including only diffusion, so that $\langle\tau\rangle$ is clearly longer for this case. This is expected, as inward diffusing CR scattering centres are continuously convected outwards, making it harder for CRs to reach the inner heliosphere, and subsequently taking longer to do so.

An approximate analytical solution for $\langle\tau\rangle$ can be derived by assuming a CR scattering centre originally located at $r = R$. Eq. 5.9 gives the average propagation time of the scattering centre to reach $r = 0$ when only diffusion is considered. The average velocity at which the scattering centres diffuse inwards, covering a distance R, is then

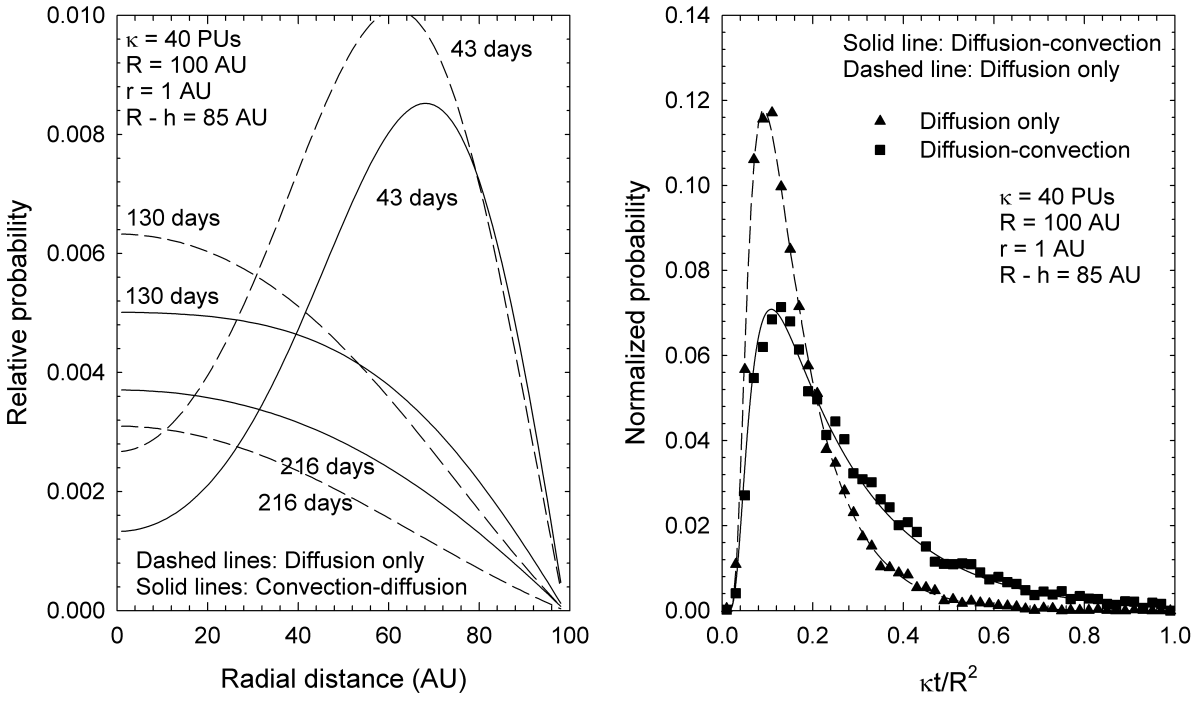

Figure 5.4: The left panel shows the numerically calculated $w(r,t)$ as a function of radial distance varying times in days, including convection (solid lines) and neglecting convection (dashed lines) in the model for the parameters as indicated. The right panel shows $w(r,t)$ as a function of time, for the different cases, at $r = 1$ AU. The scatter points show the corresponding solutions from the SDE model.

$$\langle \vec{v}_d \rangle = -\frac{6\kappa}{R}\mathbf{e}_r. \tag{5.11}$$

If outward convection with a speed of V_{sw} is also considered, the net transport velocity is then

$$\langle \vec{v}_{cd} \rangle = V_{sw}\mathbf{e}_r - \frac{6\kappa}{r}\mathbf{e}_r. \tag{5.12}$$

To be displaced by $-R\mathbf{e}_r$, the scattering centre will thus take a time

$$\langle \tau_{cd} \rangle = \frac{R^2}{6\kappa - V_{sw}R}. \tag{5.13}$$

Introducing the characteristic convection time as

$$\langle \tau_c \rangle = \frac{R}{V_{sw}}, \tag{5.14}$$

i.e. the time it takes for a scattering centre to be transported from $r = 0$ to $r = R$ without undergoing diffusion, Eq. 5.13 can be rewritten more compactly as

$$\langle \tau_{cd} \rangle = \left[\frac{1}{\langle \tau_d \rangle} - \frac{1}{\langle \tau_c \rangle} \right]^{-1}, \tag{5.15}$$

giving the approximate propagation time in the convection-diffusion model. Note that when $\langle \tau_c \rangle \to \infty$, $\langle \tau_{cd} \rangle \to \langle \tau_d \rangle$ and when $\langle \tau_c \rangle \to \langle \tau_d \rangle$, $\langle \tau_{cd} \rangle \to \infty$, i.e. when the convective and diffusive processes are in equilibrium, a CR will remain at a radial position $0 < r < R$ indefinitely. When $\langle \tau_c \rangle < \langle \tau_d \rangle$ (equivalently, $\langle v_d \rangle < \langle v_c \rangle$) the CR will be convected to $r > R$ and cannot spend any time in the heliosphere. From Eq. 5.15, this situation occurs when $\langle \tau_{cd} \rangle < 0$.

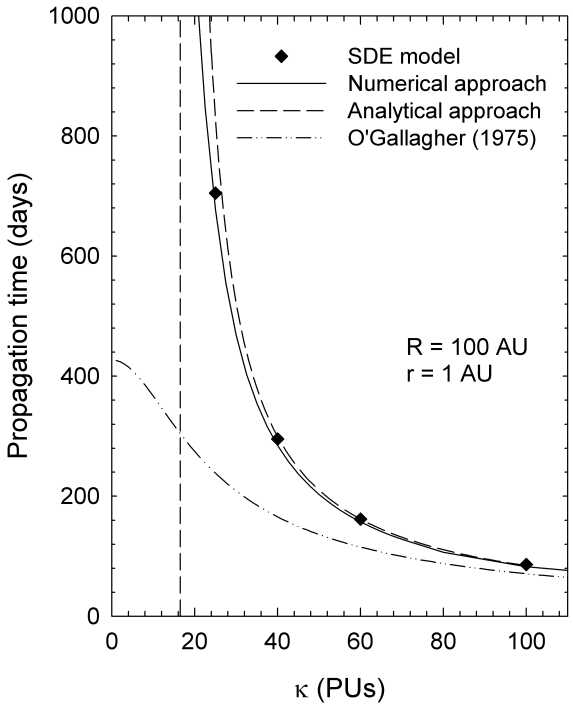

Figure 5.5: The propagation time as a function of κ for the convection-diffusion model. Scatter points show results of the SDE model, the solid line of the numerical probability wave approach, the dashed line the derived analytical solution given by Eq. 5.15 and the dashed-dotted line the analytical solution of *O'Gallagher* [1975].

In the right panel of Fig. 5.4, the resulting propagation times calculated with the SDE model are compared to the results from the probability wave model. These calculations use $\kappa = 40$ PUs and $V_{sw} = 400$ km.s^{-1} with the propagation times shown for the cases when solar wind convection is included or neglected. Again, very good agreement is obtained between the different approaches.

In Fig. 5.5, $\langle \tau \rangle$ is shown as a function of κ, with the effects of convection included. The scatter points show results from the SDE model and the solid lines $\langle \tau \rangle$ as calculated from the numerical wave probability approach. The dashed line shows $\langle \tau_{cd} \rangle$, calculated from Eq. 5.15, while the dash-dotted line shows $\langle \tau \rangle$ as calculated by *O'Gallagher* [1975]. The vertical dashed line shows the value of κ where $\langle \tau_{cd} \rangle \to \infty$. For larger values of κ the analytical approximation

of the previous section seems reasonable, whereas small deviations occur at lower values of κ. The analytical solution of *O'Gallagher* [1975], however, deviates completely from the results of the SDE model with $\langle \tau_{cd} \rangle \rightarrow \langle \tau_c \rangle$ as $\kappa \rightarrow 0$; a non-physical situation for galactic CRs in the heliosphere.

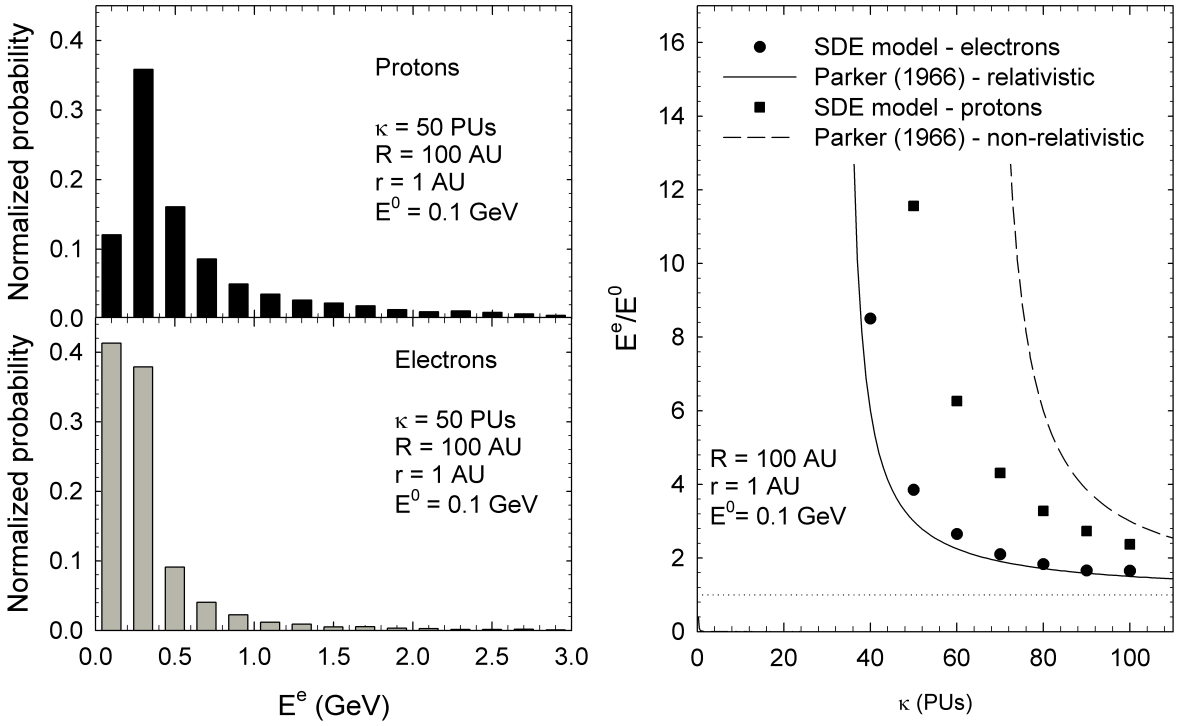

Figure 5.6: The normalized probability of E^e from the SDE model for 10000 pseudo-particles are shown in the left panel; the top panel for protons and the bottom panel for electrons. The scatter point in the right panel shows $\langle E^e/E^0 \rangle$ as a function of κ, as calculated from the SDE model. The solid line is the analytical approximation of Eq. 5.26 for relativistic CRs, the dashed line for non-relativistic CRs and the horizontal dotted line shows the limiting case of $\langle E^e/E^0 \rangle = 1$.

In his original derivation of the TPE, *Parker* [1965] derived the CR energy loss term as

$$\Im = -\frac{\partial}{\partial E}\left(\frac{\partial E}{\partial t} f\right), \tag{5.16}$$

where

$$\frac{\partial E}{\partial t} = -\frac{1}{3}\left(\nabla \cdot \vec{V}_{sw}\right) \Gamma E = -\frac{1}{3r^2}\frac{\partial}{\partial r}\left(r^2 V_{sw}\right) \Gamma E \tag{5.17}$$

is the rate at which CRs are adiabatically cooled in the expanding solar wind and f the CR distribution function. Here,

$$\Gamma = \frac{E + 2E_0}{E + E_0}, \tag{5.18}$$

with E_0 the rest energy. For this work, the focus is on galactic electrons and protons. CR electrons are highly relativistic for all energies considered, so that $E \gg E_0$ and $\Gamma \rightarrow 1$. Galactic protons of $E > 100$ MeV are, however, somewhere in between a totally relativistic and totally non-relativistic case. For fully non-relativistic CRs, $E \ll E_0$ and $\Gamma \rightarrow 2$. As pointed out by e.g. *Fisk* [1979], $\nabla \cdot \vec{V}_{sw}$ is the rate at which a solar wind volume element expands as it moves radially outwards with a speed of V_{sw}. Eq. 5.16 is derived by assuming that adiabatic cooling is the only mechanism responsible for CR energy losses. In terms of momentum, the average deceleration rate is

$$\langle \dot{p}' \rangle = \langle \frac{dp}{dt} \rangle' = -\frac{p'}{3r^2} \frac{\partial}{\partial r} \left(r^2 V_{sw} \right). \tag{5.19}$$

However, as discussed by e.g. *Webb and Gleeson* [1979], this rate is only valid if the CRs are described with respect to a frame co-moving with the solar wind at a speed of V_{sw}. In a co-ordinate system fixed on the Sun (heliocentric coordinates), the momentum loss rate has the form

$$\langle \dot{p}' \rangle = -\frac{p'}{3} \vec{V}_{sw} \cdot \vec{g}_r, \tag{5.20}$$

[e.g. *Webb and Gleeson*, 1979] where $\vec{g}_r$ is the radial CR differential intensity gradient. Although these momentum loss rates differ from one another, the resulting TPE remains unchanged, largely because of the Compton-Getting factor [e.g *Gleeson and Axford*, 1968; *Forman*, 1970; *Webb and Gleeson*, 1980].

To calculate the total energy lost by CRs propagating through the helioshere, the analytical approach of *Parker* [1965]; *Parker* [1966] and *Jokipii and Parker* [1970] is used, where the differential intensity, $j(r, E, t)$ in terms of kinetic energy, is obtained by deconvolving the equation

$$w(r, t) = \int_0^\infty j(r, E, t) dE. \tag{5.21}$$

This model introduces a constant stream of particles at $r = R$ with an energy of E^e, and calculates the average energy $\langle E^0 \rangle$ of the particles reaching $r = 0$, as

$$\langle E^0 \rangle = \frac{\int_0^{E^e} E j(0, E, t) dE}{\int_0^{E^e} j(0, E, t) dE} \tag{5.22}$$

with

$$\frac{E^e}{\langle E^0 \rangle} = \langle \frac{E^e}{E^0} \rangle \tag{5.23}$$

the average fractional energy loss. In the limit of

$$\frac{RV_{sw}}{\kappa} \ll 1, \tag{5.24}$$

Eq. 5.22 was solved by *Parker* [1966] to give

$$\langle E^0 \rangle - E^e = -\frac{\Gamma}{3} E^e \frac{RV_{sw}}{\kappa}, \tag{5.25}$$

or in terms of the fractional energy loss as

$$\langle \frac{E^e}{E^0} \rangle = \left(1 - \frac{\Gamma}{3}\frac{RV_{sw}}{\kappa}\right)^{-1}, \tag{5.26}$$

satisfying the limiting case of $\langle E^e/E^0 \rangle \rightarrow 1$ when $\kappa \rightarrow \infty$, i.e. for very large values of κ the CRs will lose no energy.

In the time backwards SDE approach used here, CRs are introduced at $r = 1$ AU with an energy of E^0. They then propagate towards the outer heliosphere, continually gaining energy adiabatically, and reach the HP with an energy of $E^e > E^0$. In this section, the SDE model incorporates convection and uses a value of $E^0 = 0.1$ GeV. The left panel of Fig. 5.6 shows binned values of E^e for 10000 individual pseudo-particles; the top panel for protons and the bottom panel for electrons. As expected, $E^e > E_0$, with no apparent upper limit to the fractional energy loss. The expectation value $\langle E^e/E^0 \rangle$ is calculated, and shown as a function of κ in the right panel of the figure as scatter points. As expected, the fractional energy loss increases with decreasing values of κ. The solid line shows the analytical approximation of Eq. 5.26, for relativistic CRs ($\Gamma = 1$), the dashed line the same approximation but for non-relativistic CRs ($\Gamma = 2$), while the horizontal dotted line shows the limiting case of $\langle E^e/E^0 \rangle = 1$. The SDE electron solutions and the $\Gamma = 1$ approximation agree quite well. For protons, the fractional energy loss is expected to be somewhere in between the $\Gamma = 1$ and $\Gamma = 2$ approximations, and this is indeed what the SDE model gives. These good comparisons between the results indicate the validity of the SDE approach in calculating the energy losses suffered by CRs.

5.4 Electrons and Protons in Three Dimensions

Using the 3D SDE modulation model, energy spectra at Earth are shown in Fig. 5.7 for galactic electrons (left panel) and protons (right panel). For galactic CRs, this is assumed to be the HP, where their intensities are prescribed by a CR species specific LIS. For electrons the LIS of *Langner et al.* [2001] is used, while for protons the LIS of *Moskalenko et al.* [2002] is used. Using a *Parker* [1958] HMF, solutions are shown for both the $A < 0$ (left panel) and $A > 0$ (right panel) HMF polarity cycles, illustrating the effect of gradient and curvature drifts in the model. The drift velocity is incorporated into the model as discussed by *Strauss et al.* [2011a], which includes curvature, gradient and neutral sheet drifts. For the latter, a flat current sheet

drift model is adopted, while the parallel diffusion coefficient is assumed to have the following form

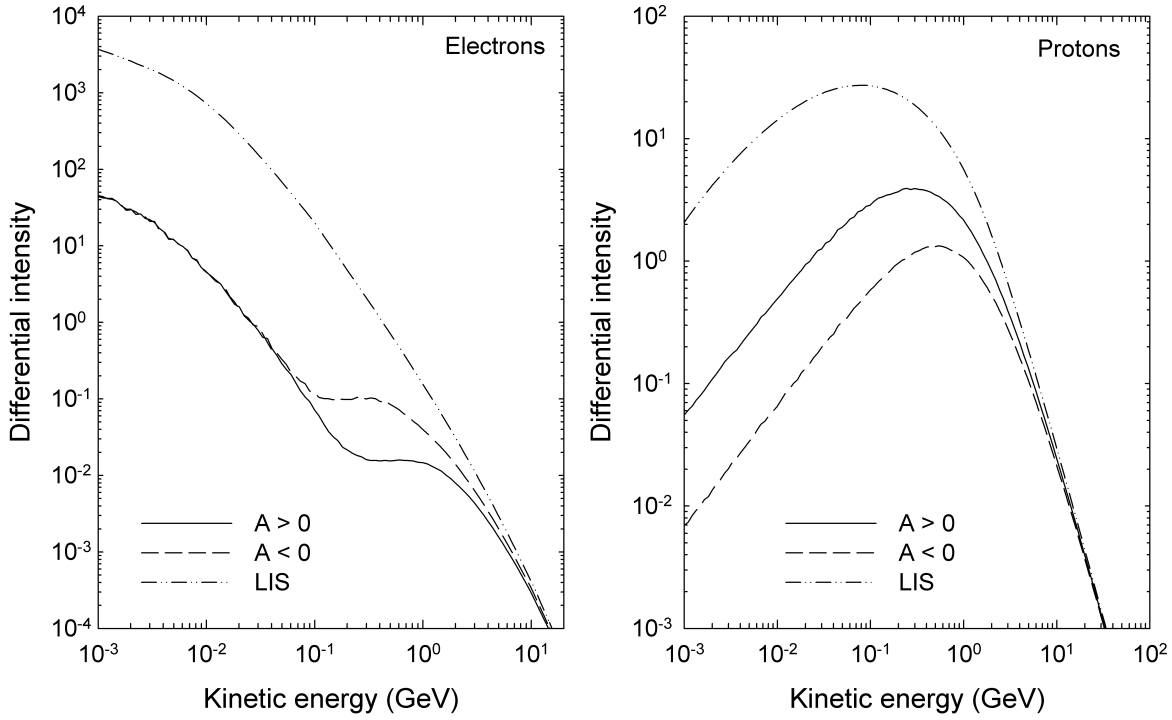

Figure 5.7: Modelled energy spectra at Earth, with respect to the LIS at $R = 120$ AU, for galactic electrons (left panel) and protons (right panel) for both HMF polarity cycles, indicated by $A < 0$ and $A > 0$, using the 3D SDE modulation model.

$$\kappa_{||} = \kappa_0 \frac{P}{P_0} \left(1 + \frac{r}{r_0}\right) \tag{5.27}$$

with $r_0 = 1$ AU, $P_0 = 1$ GV and $\kappa_0 = 25$ PUs for protons and electrons above 1 GV. Below 1 GV, an energy independent $\kappa_{||}$ is used for electrons, with $P/P_0 \equiv 1$. Furthermore, isotropic perpendicular diffusion with $\kappa_{\perp r} = \kappa_{\perp \theta} = 0.02\kappa_{||}$ [*Giacalone and Jokipii*, 1999] is assumed. The diffusion tensor is thus qualitatively similar to the one used by *Potgieter and Moraal* [1985].

Analytical approximations of CR energy losses in the spatially 3D scenario are impossible and must thus be studied with numerical modulation models. The traditional way of computing this is shown for illustrative purposes in Fig. 5.8: At the HP, a near Gaussian input spectrum is specified. This input spectrum is then modulated, with the resulting distribution at Earth investigated. In Fig. 5.8, nine of these peaks are introduced at the HP for electrons (left panel) and protons (right panel). The corresponding modulated distributions at Earth are also shown (with the numbers labelling the individual pairs of solutions), with the intensities normalized at the HP to LIS levels. Examining how these initial peaks modulate, gives some indication of the energy losses suffered by the CRs. Normally, only the shift in energy of the peak's maximum intensity is taken as the energy loss, i.e. for protons, peak 7 is introduced at the HP

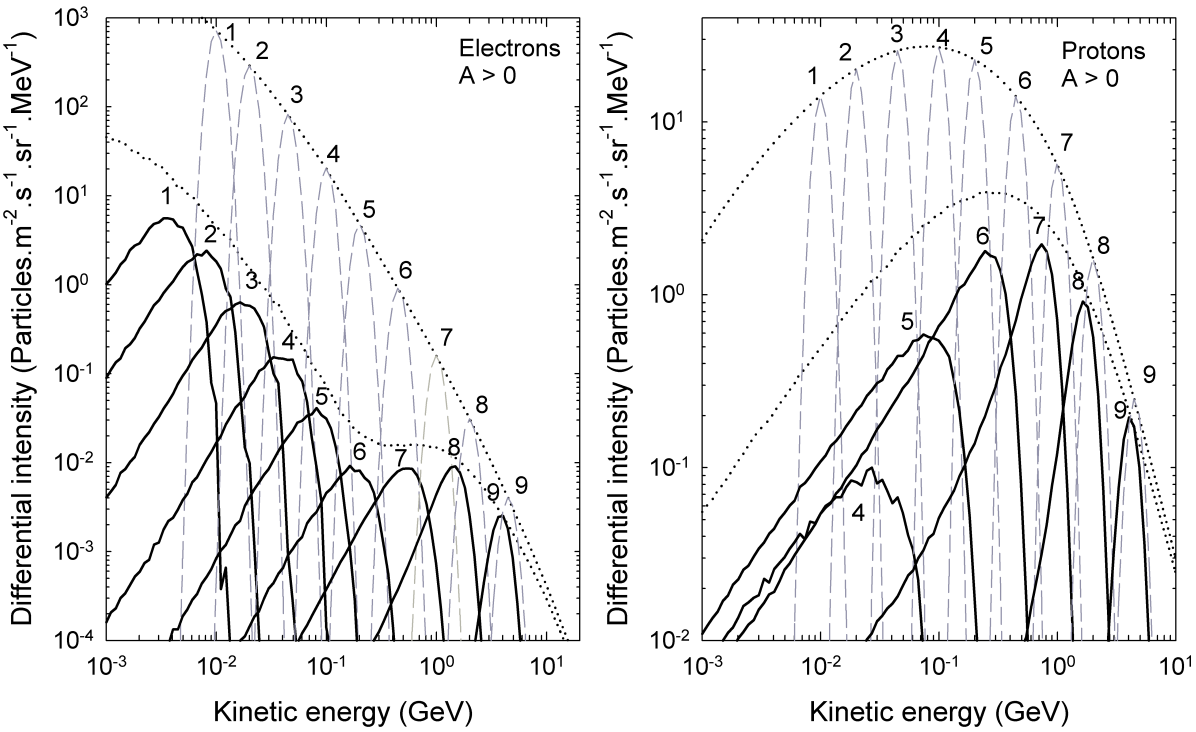

Figure 5.8: Modelled energy spectra at Earth for electrons (left panel) and protons (right panel) for the $A < 0$ HMF cycle using the 3D SDE model to illustrate the total effect of adiabatic energy losses under these drift conditions. Instead of a continuous function for the LIS, Gaussian peaks are specified at different energies (dashed grey lines), while the resulting spectra at Earth (for each of the numbered peaks independently) are shown as the solid lines. The dotted lines are the corresponding LIS and modulated solutions from the previous figure.

with $E \approx 1$ GeV, while it ends up at Earth at $E \approx 0.5$ GeV, giving an energy loss of $\Delta E \approx 500$ MeV. This however does not give the entire picture as the modulated intensities at Earth, as all of the peaks have a long *tail* distribution to lower energies. Characteristic of adiabatic cooling, proton spectra at Earth follow a $j \propto E$ spectrum at low energies, while electrons follow a $j \propto E^2$ trend [see e.g. *Moraal and Potgieter*, 1982]. To calculate the *true* energy loss, the energy densities of both the peaks and their counterparts at Earth, have to be integrated and the total energy density calculated. As demonstrated in the previous sections, the SDE approach does not have this limitation because the energy losses can be calculated directly for each pseudo-particle.

A good test for the calculated τ and ΔE is illustrated in Fig. 5.9. Above 1 GV, all transport coefficients for protons and electrons (as used in this study) are assumed to be exactly the same. The propagation times and rigidity loss of protons and electrons (in opposite drift cycles for the oppositely charged CRs) above 1 GV should thus be identical; a fact illustrated in Fig. 5.9. The figure shows the rigidity loss (keeping in mind that the rigidity loss rate is independent of Γ) as a function of the propagation time at 5 GV and 10 GV and different drift cycles. It can thus be summarized that protons and electrons, at the same rigidity, will lose the same amount

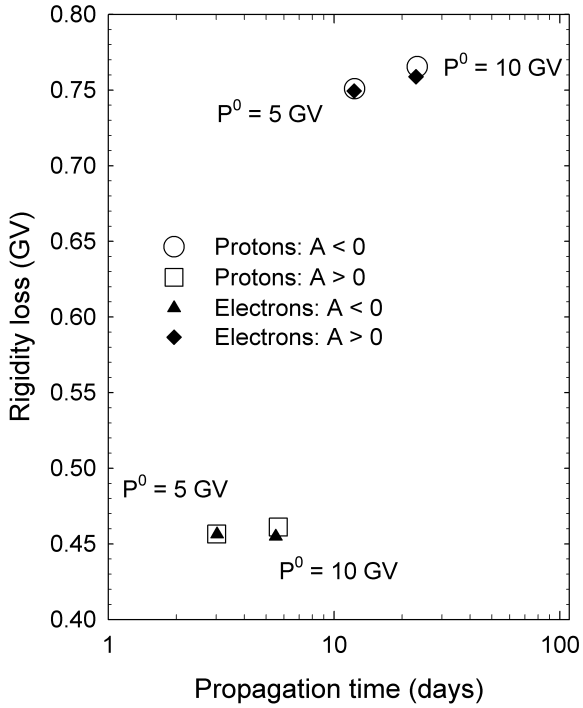

Figure 5.9: The rigidity loss of CR electrons and protons, plotted as a function of propagation time for $P^0 = 5$ GV and 10 GV and the two polarity cycles.

of rigidity adiabatically and have identical propagation times, if they had identical transport (drift and diffusion) coefficients.

The modelled energy losses and propagation times of protons (top panels) and electrons (bottom panels) are shown in Fig. 5.10 as a function of energy (E^0) for both the $A > 0$ (left panels) and $A < 0$ (right panels) HMF polarity cycles. In contrast to the results of the previous sections, the 3D scenario is much more complex because of the addition of an energy dependent diffusion tensor and CR drifts. Focusing firstly on protons, for both drift cases the propagation time decreases with increasing energy, as expected, because both the diffusion tensor and drifts increase with energy (rigidity). The propagation time are also much larger in the $A < 0$ than the $A > 0$ cycle. This is consistent with general drift considerations: For the $A < 0$ cycle, the protons that reach Earth have to drift inwards along the HCS, taking a much longer time to reach Earth than protons which simply drift towards Earth from the polar regions in the $A > 0$ cycle. The energy losses suffered by the protons also decrease with increasing energy and is also larger for the $A < 0$ drift scenario. For electrons, the propagation times are qualitatively similar to those of the protons. The propagation time, $\langle\tau\rangle$, decreases with energy and is larger for the $A > 0$ case (i.e. the drift cycle when electrons drift inward along the HCS). More intriguing is the fact that τ is much larger for electrons than protons at the same energy. For protons and electrons at the same energy, the rigidity of the protons is much higher, and as the transport coefficients are expressed in terms of rigidity, the protons will have a much

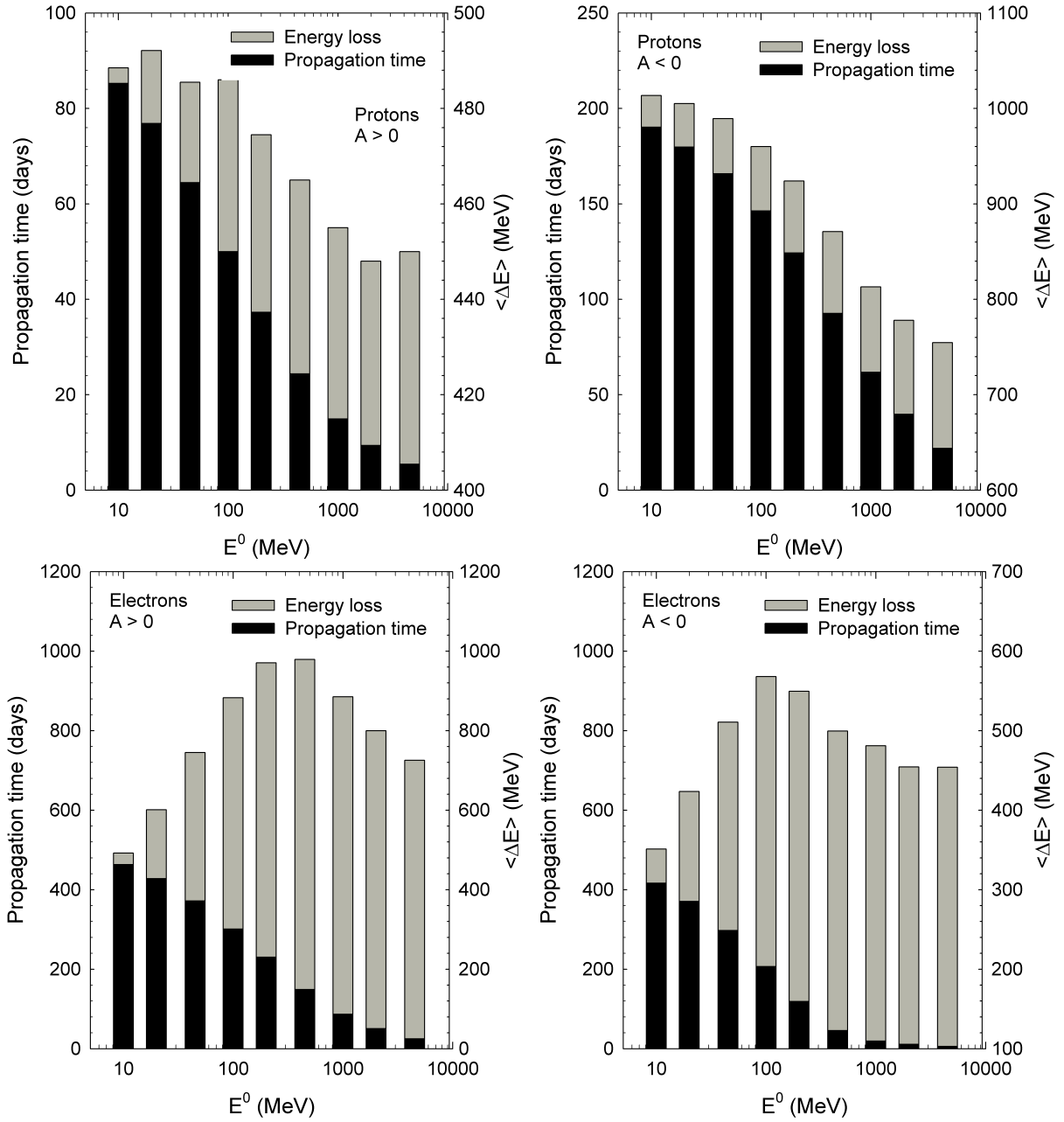

Figure 5.10: Calculated propagation times $\langle\tau\rangle$ and energy losses $\langle\Delta E\rangle$ of protons (top panels) and electrons (bottom panels) are shown for the $A > 0$ (left panels) and $A < 0$ (right panels) HMF polarity cycles. The propagation times are shown as black fills, while energy losses are indicated by grey fills.

larger mean free path and drift speed, and thus propagate faster than the electrons. The energy losses of electrons peak at intermediate energies, and decrease at high and low energies. This decrease at low energies (being absent for the proton case) is due to the electron diffusion coefficients being energy independent below $E \approx 1$ GeV. Electrons at e.g. 10 MeV and 100 MeV will thus have the same diffusion coefficient, but the 100 MeV particles will lose more energy, as the energy loss rate is proportional to E. More noteworthy is that the energy losses

of electrons (at least at 100 MeV) are comparable to those of the protons. This is in contrast to the widely believed paradigm that electrons lose relatively little energy adiabatically [e.g. *Langner and Potgieter*, 2004a; *Nkosi et al.*, 2008]. This paradigm is based on the absence of the adiabatic limit $j \propto E^2$ in electron spectra observed and modelled at Earth. As however discussed by *Moraal and Potgieter* [1982], this limit will only be seen when the net CR streaming is negligible; something that is more difficult to satisfy for electrons than protons. It might seem contradictory that electrons have longer propagation times than protons, yet lose equivalent amounts of energy adiabatically. One must, however, keep in mind that the energy loss rate is also proportional to Γ (see Eq. 5.17), and that Γ is always larger for protons (for the energies considered here) than for electrons (see also the right panel of Fig. 5.6). This again illustrates the difficulty in calculating and interpreting the energy losses suffered by CRs.

5.5 Summary and Conclusions

The propagation times and energy losses of CRs in the supersonic solar wind were calculated by making use of an SDE numerical modulation model with increasing complexity.

First, the propagation times τ of CRs were calculated, for a spatially 1D scenario, with and without solar wind convection included in the model. These results were then compared successfully to analytical approximations, vindicating the SDE approach. The results indicate that τ is highly dependent on κ, as expected, and is generally longer when solar wind convection is included in the model, as CRs find it more difficult to penetrate to the inner heliosphere. For the aforementioned scenario, the analytical approximations of *O'Gallagher* [1975] seem to be insufficient to describe τ. The reason for this is that he used the approximation $\kappa \ll 1$, a non-physical assumption, because at these very small values of κ, convection dominates the diffusive process and CRs are unable to enter the heliosphere. The fractional energy loss of CRs was calculated, for the spatially 1D case, and also compared successfully to analytical approximations. As with τ, the energy loss increases with a decrease of κ. It was also demonstrated that the energy loss of non-relativistic CRs is much larger than for relativistic particles, due to the dependence on Γ (Eq. 5.17) of the energy loss rate.

With the SDE model thoroughly benchmarked, τ and ΔE (the average energy loss) were calculated for CR electrons and protons, for a spatially 3D scenario. The calculated values again depend strongly on the assumed transport (diffusion and drift) coefficients, with the choices of these parameters leading to τ decreasing with increasing energy. The drift cycle dependence of τ was also illustrated, with CRs having longer propagation times in the HMF cycle when they drift inward along the HCS towards Earth. It is found that τ is much larger for electrons than for protons at the same energy, as the electrons have a smaller mean free path (above rigidities of 1 GV for this choice of the diffusion tensor). The energy loss ΔE for protons also decreases with increasing energy and is largest in the $A < 0$ drift cycle. Due to the assumed energy independence of $\mathbf{K}$ for electrons in this energy range, it was however found that ΔE decreases

at low energies. Moreover, ΔE for electrons is smaller than for protons with the same energy, but larger than previously thought.

In contrast to previous studies [e.g. *Gervasi et al.*, 1999], it is not stated here that $\Delta E \propto \tau$. Referring back to Eq. 5.17, this will only be the case when the energy loss rate (in the solar wind frame) is constant. The energy loss rate is however dependent on Γ, which is energy dependent, as well as E itself, making the process per definition non-linear. Besides, it is also dependent on the quantity $\nabla \cdot \vec{V}_{sw}$. In this work the focus was on the supersonic solar wind inside the TS, where $\nabla \cdot \vec{V}_{sw} > 0$, and adiabatic cooling consequently occurs. In the heliosheath, however, a mixture of $\nabla \cdot \vec{V}_{sw} > 0$, $\nabla \cdot \vec{V}_{sw} = 0$, and $\nabla \cdot \vec{V}_{sw} < 0$ can occur. When $\nabla \cdot \vec{V}_{sw} < 0$, adiabatic heating of CRs can take place [e.g. *Langner et al.*, 2006] and Eq. 5.17 changes to an energy gain rate. When $\nabla \cdot \vec{V}_{sw} = 0$, no adiabatic energy changes can occur, even in the limit when $\tau \rightarrow \infty$.

Comparing the energy losses that CRs experience inside the heliosphere as calculated with a SDE model, which includes CR drifts, with previous modelling results [e.g. *Potgieter and Moraal*, 1985], remarkably good agreement is found for both HMF polarity cycles. In addition, the SDE approach offers an exact method for calculating energy losses, directly from the numerical scheme, in a full 3D heliosphere, for which no analytical solutions are possible. The same applies to the calculation of the CR propagation times with the SDE approach. Compared to ADI-based modulation models, the SDE approach gives significant additional insights into the modulation process, in particular into a subtle process such as adiabatic energy losses as described above.